

Ultrasmall PtNi Bimetallic Nanoclusters for Oxygen Reduction Reaction in Alkaline Media

Wei He^{1,*}, Wen Wu² and Zhenghua Tang^{2,3,*}

¹ Chongqing Chemical Industry Vocational College, Chongqing, 401220, P. R. China.

² Guangzhou Key Laboratory for Surface Chemistry of Energy Materials, New Energy Research Institute, School of Environment and Energy, South China University of Technology, Guangzhou Higher Education Mega Centre, Guangzhou, 510006, China.

³ Guangdong Provincial Key Laboratory of Atmospheric Environment and Pollution Control, Guangdong Provincial Engineering and Technology Research Center for Environmental Risk Prevention and Emergency Disposal, School of Environment and Energy, South China University of Technology, Guangzhou, Guangdong, 510006, P. R. China

*E-mail: 2215432511@qq.com, zhht@scut.edu.cn

Received: 12 February 2018 / Accepted: 13 March 2018 / Published: 10 April 2018

Ultrasmall PtNi bimetallic nanoclusters (NCs) were synthesized and employed as effective electrocatalysts for oxygen reduction reaction (ORR). PtNi NCs capped by polyvinyl pyrrolidone were synthesized through a wet chemical approach with optical property examined by UV-visible absorbance. The surface micro-structure and electronic structure of these bimetallic NCs were measured by transmission electron microscopy (TEM), X-ray photoelectron spectroscopy (XPS), and other techniques. The bimetallic PtNi NCs demonstrated effective activity toward ORR in alkaline electrolyte and their electrocatalytic properties were modulated by the variation of Pt-to-Ni ratio. Among the series of samples tested, Pt₆₇Ni₃₃ NCs exhibited the best activity, superior than monometallic nickel nanoparticles, platinum nanoclusters and other alloyed samples, within the terms of onset potential, kinetic current density and durability. Pt₆₇Ni₃₃ NCs exhibited almost identical specific activity but markedly higher long-term durability than commercial Pt/C. The method here may provide a generic approach for fabricating ultrasmall bimetallic alloyed nanoclusters with extraordinary activity and desirable stability for ORR.

Keywords: PtNi nanoclusters; Alloy; Fuel cell; Electrocatalyst; Oxygen reduction reaction

1. INTRODUCTION

Proton exchange membrane fuel cell (PEMFC) has been widely considered as one of the most promising alternatives for future energy provision.[1-3] Despite much research has been done, the lack of high-performance catalysts for oxygen reduction reaction (ORR) occurring at the cathode still

remains a bottleneck to fully realize the potentials of PEMFC.[4, 5] Currently, the most widely employed catalyst for ORR is Pt-based hybrid nanomaterials.[6-12] For instance, small Pt nanoparticles supported on black carbon (Pt/C) have been well recognized as the state-of-the-art electrocatalyst. However, Pt is a noble metal with high price and very limited earth abundance. Therefore, to maximally realize the potential of Pt elements is crucial to enhance the catalytic activity and of vast practical value.[13, 14]

One strategy to lower the Pt content is introducing transitional metal into the catalyst, that is, Pt alloyed electrocatalyst for ORR.[15-18] Note that, Pt alloys with transitional metals such as PtNi,[19, 20] PtCo,[21, 22] PtCu,[23] PtFe,[24] PtCr[25] have been reported to possess higher ORR activity than commercial Pt/C. Specifically, some of these PtM electrocatalyst demonstrated markedly higher specific activity and mass activity as well as enhanced stability. Fundamental investigations of well-defined metal surface have confirmed that the modified electronic structure of Pt in the alloys plays a key role in enhancing the electrocatalytic activity.[26, 27]

Among the PtM series, the development of PtNi electrocatalyst have been attracting continuous research attentions ever since the discovery was made in 2007 in which the Pt₃Ni(111) crystal surface was able to exhibit a remarkably high ORR activity of 18 mA/cm² with regard to Pt.[28] Zhang and co-workers examined the shape effects toward ORR of Pt₃Ni nanocrystals, and found that the (111)-facet terminated nano-octahedra was significantly more active than the (100)-facet bounded nanocubes.[29] Homogeneous PtNi nanoparticles were prepared by an organic solvothermal approach and cast on carbon with high surface area, and such hybrid materials exhibited 2-3 folds of ORR activity compared with Pt/C.[30] By employing a facile surfactant-free solvothermal method, Strasser group synthesized octahedral PtNi nanoparticles with about 10 times ORR activity gains in both Pt specific and mass activity.[19] Recently, Huang and co-workers demonstrated that transitional metal-doped Pt₃Ni octahedra supported on carbon exhibited an incredibly high specific and mass activity, which were 81 and 73-fold enhancements compared with commercial Pt/C, respectively.[31] Moreover, vertically aligned PtNi alloyed nanorods have been fabricated using glancing angle deposition technique and ORR area-specific activity enhancement was observed.[32] Peng group developed a scalable, surfactant-free and cost-effective method for producing octahedral PtNi alloyed nanoparticles on carbon support.[33] Recently, Eid and co-workers successfully demonstrated a facile and straightforward method for the scalable preparation of porous dendritic PtNi nanocrystals as efficient catalysts for ORR.[34]

Interestingly, all these advances have been achieved on PtNi nanomaterials with relatively large dimensions. Attentions regarding small sized PtNi nanoclusters have been rarely gained. Note that, nanocluster is a novel type of nanoparticle with ultrasmall dimension, and normally possesses unique optical, physiochemical and electrochemical properties due to the quantum confinement effects.[35-37] Moreover, thanks to their small size dimension, exceptional catalytic activity has been found in a variety of catalytic reaction including CO oxidation,[38] selective hydrogenation[39] as well as ORR for Pt nanoclusters.[40, 41] Albeit these progress in small Pt nanoparticles and/or clusters, alloyed Pt clusters hold great potential as catalyst for electrocatalytic reaction which urges for more research efforts.

In this study, PtNi alloyed nanoclusters were synthesized and employed as effective electrocatalyst for ORR. The surface micro-structure and electronic structure of these bimetallic NCs were measured by TEM, XPS, and other techniques. The bimetallic PtNi NCs demonstrated effective activity toward ORR in alkaline media and their electrocatalytic properties were modulated by the variation of Pt-to-Ni ratio. Among a series of samples tested, Pt₆₇Ni₃₃ NCs exhibited the best activity, superior than monometallic nickel nanoparticle, platinum nanoclusters and other alloyed samples, within the terms of onset potential, kinetic current density and durability. Notably, Pt₆₇Ni₃₃ NCs exhibited almost identical specific activity but markedly higher long-term stability than Pt/C.

2. MATERIALS AND METHODS

2.1. Materials

Chloroplatinic(III) acid hexahydrate (H₂PtCl₆·6H₂O, 99%) was bought from Aladdin industrial Corporation (Shanghai, China), nickel(II) chloride (NiCl₂·6H₂O, 98%) and glycol were acquired from Damao Chemical Industry (Tianjin, China), PVP (K-30, MW= 40, 000) was purchased from Energy Chemicals (Shanghai, China). Sodium hydroxide and 20 wt% Pt/C was purchased from Sinopharm Chemical Reagents Co., Ltd. and Alfa Aesar, respectively. Water was provided by a Barnstead Nanopure Water System (18.3 MΩ·cm). All chemicals were used as received.

2.2. Synthesis of PtNi bimetallic nanoclusters (PtNi NCs)

The PtNi bimetallic NCs were prepared by following a modified reduction method.[42, 43] The typical synthesis of Pt₆₇Ni₃₃ NCs were described as follows: PVP (0.4006 g, 3.57 mmol) and nickel(II) chloride (NiCl₂·6H₂O, 20.2 mg, 0.085 mmol) were first co-dissolved in 60 mL of glycol at 80 °C. Then the aqueous solution of H₂PtCl₆·6H₂O (85.4 mg, 0.165 mmol) was added into the above solution at 0-5 °C, and the pH was adjusted to 9-11 by dropwise addition of sodium hydroxide (NaOH, 1 M). The mixture was stirred and refluxed at 198 °C for 3 h with a nitrogen flow. The color changed from faint yellow to dark brown gradually in the first half an hour. For other PtNi NCs with different Pt-to-Ni ratios, the total metal amount was kept as 0.25 mmol, while the amount of Pt and Ni precursors changed correspondingly. The precursor feeding ratios of Pt/Ni were 1: 0, 3: 1, 2: 1, 1: 1, 1: 2, and 0: 1, which were denoted as Pt₁₀₀, Pt₇₅Ni₂₅, Pt₆₇Ni₃₃, Pt₅₀Ni₅₀, Pt₃₃Ni₆₇, and Ni₁₀₀, respectively. The obtained NCs were dialyzed for 2 days through a semi-permeable membrane with a MWCO (Molecular weight cutoff) of 40, 000 Da. After the solvents were removed by rotary evaporator, the as-obtained solids were pure bimetallic NCs.

2.3. Characterizations

UV-visible absorbance was acquired with a Shimadzu 2600/2700 UV-visible scanning spectrophotometer using a 1 cm quartz cell. TEM micrographs were acquired with a high-resolution transmission electron microscope (JEOL JEM-2010), where samples were prepared by dropcasting a

catalyst dispersion directly onto a copper grid coated with a holey carbon film. XPS detection was performed with a VG MultiLab 2000 machine equipped with a monochromatic Al K X-ray source (Thermo Scientific).

2.4. Electrochemical tests

Electrochemical tests were conducted with a CHI 750E electrochemical workstation (CH Instruments Inc.) in a 0.1 M KOH aqueous solution at room temperature. A platinum wire was employed as the counter electrode while a Ag/AgCl electrode was used as the reference electrode. A glassy carbon disk electrode (diameter 5.61 mm) of a RRDE (with a collection efficiency of 37%, Pine Instrument, Inc.) was employed as the working electrode. It was cleaned by mechanical polishing with aqueous slurries of 0.3 μm alumina powders on a polishing cloth. The catalyst ink was prepared by adding 20 mg of a catalyst into 10.0 mL ethanol solution containing 100 μL Nafion (5 wt%, Aldrich). The catalyst ink (10 μL) was then drop-cast onto the glassy carbon disk and dried at room temperature, and the catalyst loading was calculated as 80.8 $\mu\text{g cm}^{-2}$ for the series of samples.

The electrochemical surface area (ECSA) measurements were conducted with a RRDE system in a nitrogen-saturated aqueous solution with 0.1 M HClO₄ at a rotation rate of 1600 rpm with a scan rate of 50 mV s⁻¹. In all electrochemical measurements, the Ag/AgCl reference electrode was calibrated with respect to a reversible hydrogen electrode (RHE). The calibration was conducted in a pure H₂ (99.999%) saturated electrolyte with a Pt wire as both the working electrode and counter electrode. Cyclic voltammograms were recorded at a scan rate of 10 mV/s, and the average of the two potentials where the current crossed zero was adopted as the thermodynamic potential for the hydrogen electrode reactions. In 0.1 M KOH, $E_{\text{Ag/AgCl}} = E_{\text{RHE}} + 0.966 \text{ V}$.

3. RESULTS AND DISCUSSION

3.1. HR-TEM images of the PtNi NCs

Table 1. ORR activity comparison of different samples.

Sample	E_{onset} (V)	n value	j_p (mA/cm ²)	ECSA (cm ²)	SA @0.6 V (mA/cm ²)
Pt ₁₀₀ NCs	0.83	3.5-3.7	4.4	0.52	0.43
Pt ₇₅ Ni ₂₅ NCs	0.86	3.5-3.7	4.8	0.54	0.51
Pt ₆₇ Ni ₃₃ NCs	0.92	3.6-3.7	6.5	0.67	0.61
Pt ₅₀ Ni ₅₀ NCs	0.83	3.4-3.6	3.9	0.37	0.31
Pt ₃₃ Ni ₆₇ NCs	0.83	3.3-3.5	3.5	0.21	0.17
Ni ₁₀₀ NPs	0.72	3.1-3.3	3.1	---	---
Pt/C	0.96	3.7-3.8	6.7	1.72	0.62

E_{onset} was determined from cyclic voltammograms (**Figures 3a and S4a**);

j_p was determined from rotating-disk voltammograms (**Figures 3b and S4b**);

n is the number of electron transfer (**Figures 3c and S4c**).

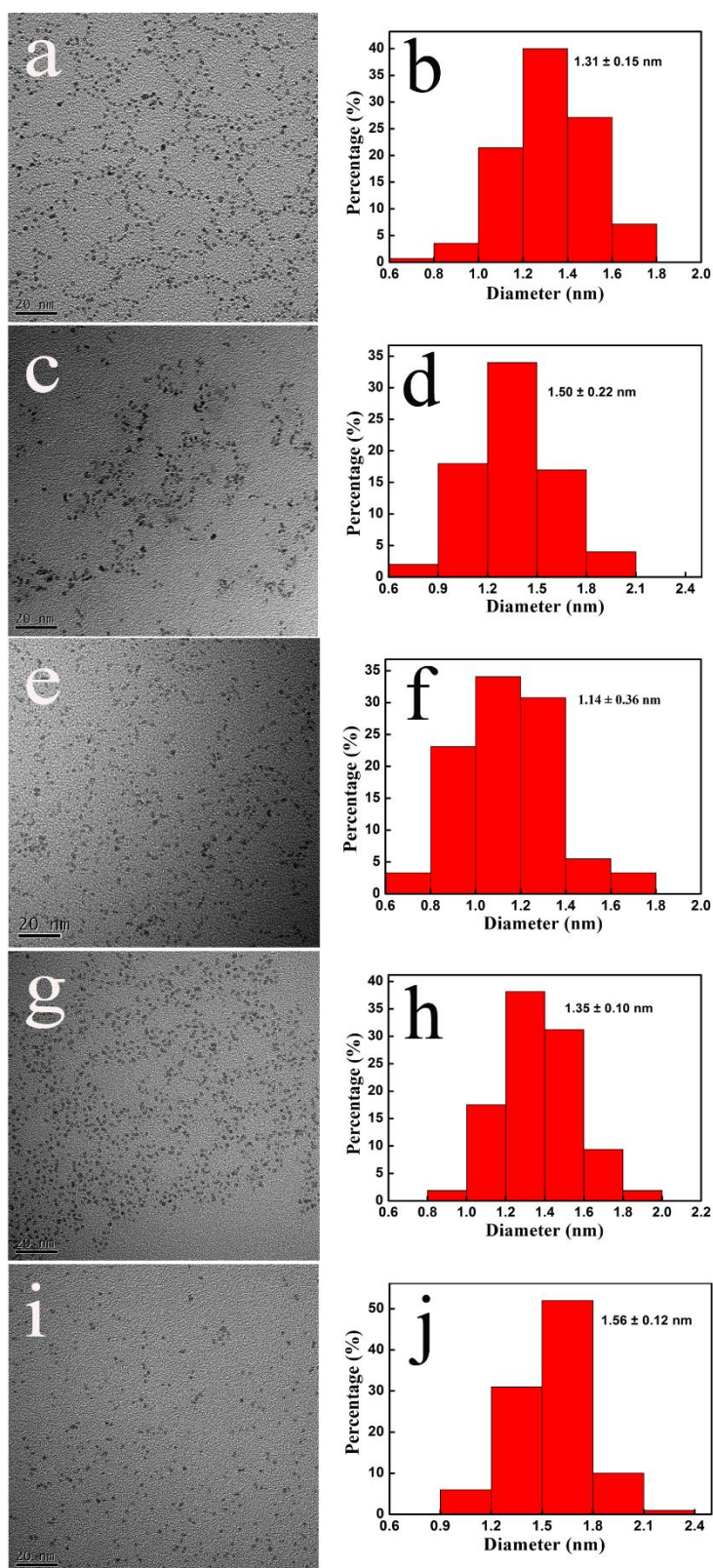


Figure 1. Typical TEM image and homologous size distribution histograms of (a, b) Pt₁₀₀ NCs, (c, d) Pt₇₅Ni₂₅ NCs, (e, f) Pt₆₇Ni₃₃ NCs, (g, h) Pt₅₀Ni₅₀ NCs, and (i, j) Pt₃₃Ni₆₇ NCs. Scale bar = 20 nm.

The PtNi alloyed NCs with different Pt-to-Ni ratios were first synthesized. As depicted in **Figure S1**, a featureless exponential decay profile in absorbance was obtained for all the samples. Such absorbance feature indicated that, bi-metallic nanoclusters with ultrasmall size probably were acquired.[36, 44] The typical TEM image of the Ni₁₀₀ sample can be found in **Figure S2**, and clearly, well defined particles with high crystalline can be observed. The average dimension (length or width) of these nickel nanoparticles is above 20 nm. Besides this sample, the representative TEM images and their corresponding size distribution histogram of the other samples are presented in **Figure 1**. One can see that, all the particles are spherical and well dispersed with good uniformity. No aggregation can be observed. Statistical analysis based on more than 100 individual particles shows that, the average diameter was estimated to be 1.31 ± 0.15 nm for Pt₁₀₀ NCs, 1.50 ± 0.22 nm for Pt₇₅Ni₂₅ NCs, 1.14 ± 0.36 nm for Pt₆₇Ni₃₃ NCs, 1.35 ± 0.10 nm for Pt₅₀Ni₅₀ NCs, and 1.56 ± 0.12 nm for Pt₃₃Ni₆₇ NCs. The results suggest that, with Ni precursor only, large nanoparticles were obtained, while besides that, ultrasmall nanoclusters with diameter less than 2 nm were acquired for Pt alone and all the PtNi alloys.

3.2. XPS analysis of the PtNi NCs

Next, the electronic structure of these PtNi NCs was further evaluated by XPS analysis. The XPS survey scan spectra of Pt₆₇Ni₃₃ NCs can be found in **Figure S3**. Sharp peaks from C1s, N1s, O1s, Ni2p and Pt4f can be easily identified. **Figure 2** presents the Pt 4f core-level XPS spectra of PtNi NCs. It has been documented that, the binding energy of Pt4f_{7/2} electrons from Pt(0) and Pt(II) is ~ 71.5 and ~ 72.3 eV, respectively.[45, 46] Clearly, the binding energy for Pt4f_{7/2} electrons of all the samples is between Pt(0) and Pt(II), indicating a valence state of Pt is (0, 2). Interestingly, with the decreasing of Pt contents in the alloyed NCs, the binding energy demonstrated a red-shift. Such binding energy decrease implies that the electron transfer occurred from Ni atoms to Pt atoms, which has been described in some previous reports for PtM (M= Fe, Co, Ni or other transition metals) alloys.[15, 17]

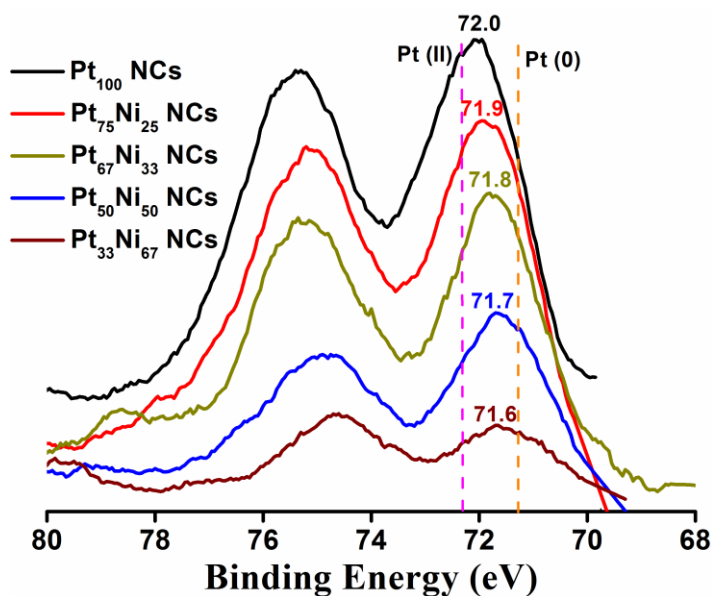


Figure 2. The Pt 4f core-level XPS spectra of Pt₇₅Ni₂₅, Pt₆₇Ni₃₃, Pt₅₀Ni₅₀, and Pt₃₃Ni₆₇ NCs.

3.3. Electrocatalytic performance toward ORR of the as-prepared PtNi NCs

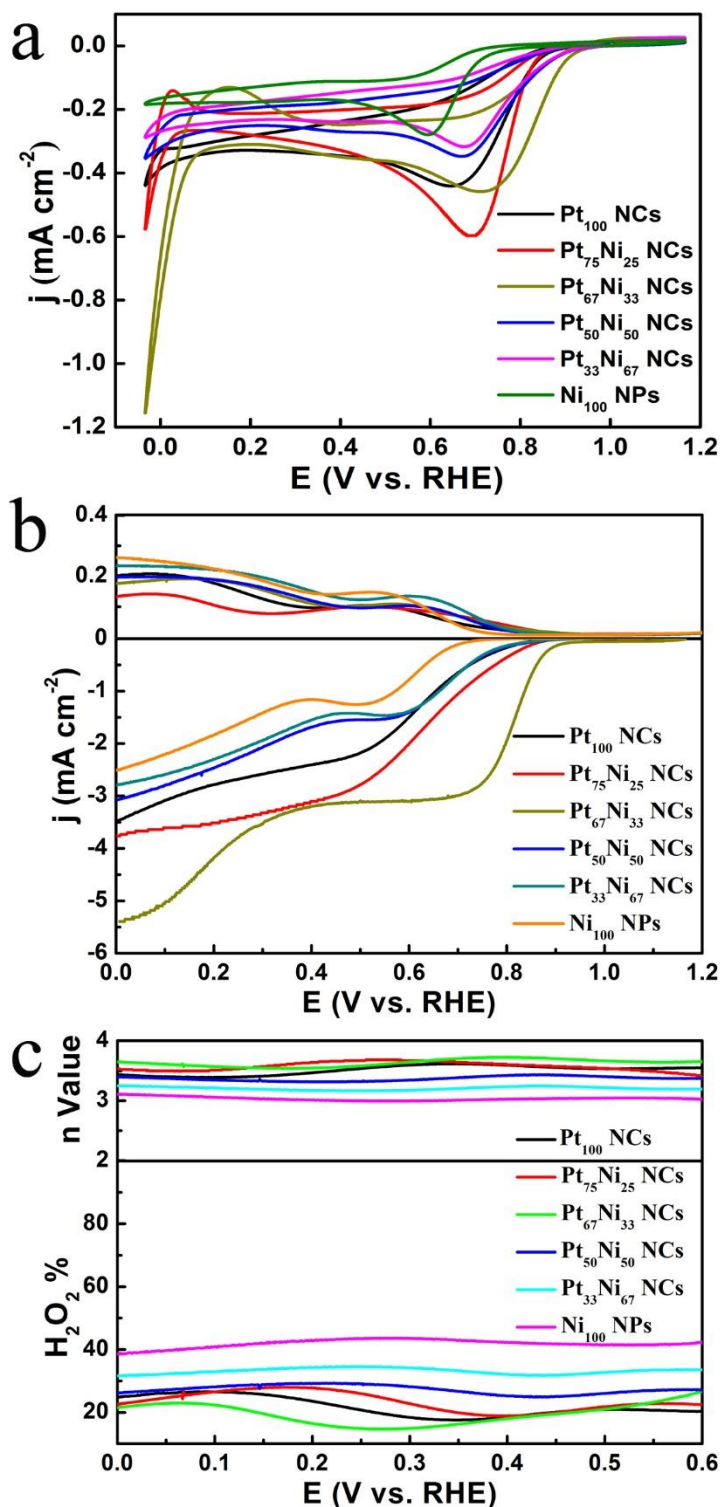


Figure 3. (a) Cyclic voltammograms, (b) RRDE voltammograms, and (c) plots of the electron transfer numbers and yields of H₂O₂ for a glassy carbon electrode modified with Pt₁₀₀ NCs, Pt₇₅Ni₂₅ NCs, Pt₆₇Ni₃₃ NCs, Pt₅₀Ni₅₀ NCs, Pt₃₃Ni₆₇ NCs, and Ni₁₀₀ NPs in O₂-saturated 0.1 M KOH solution. In panel (b), the electrode rotation rate is 2500 rpm. Potential scanning rate for all is 10 mV s⁻¹.

The as-prepared nanoclusters were then subjected to electrocatalytic activity test toward ORR. **Figure 3a** depicts the cyclic voltammograms of a glassy carbon electrode modified with 20 μg of Pt₁₀₀ NCs (black curve), Pt₇₅Ni₂₅ NCs (red curve), Pt₆₇Ni₃₃ NCs (green curve), Pt₅₀Ni₅₀ NCs (blue curve), Pt₃₃Ni₆₇ NCs (cyan curve), and Ni₁₀₀ NPs (magenta curve) in an oxygen-saturated 0.1 M KOH solution at room temperature with a potential scan rate of 10 mV s⁻¹. It can be seen that the catalytic performance varies drastically with the different Pt-to-Ni ratio in the series. For instances, the highest onset potential is 0.92 V (vs. RHE) from Pt₆₇Ni₃₃ NCs, and the onset potentials of the other samples are estimated as 0.83 V for Pt₁₀₀ NCs, 0.86 V for Pt₇₅Ni₂₅ NCs, 0.83 V for Pt₅₀Ni₅₀ NCs, 0.83 V for Pt₃₃Ni₆₇ NCs, and 0.72 V for Ni₁₀₀ NPs. Moreover, the cathodic peak potential also exhibits a distinct variation at 0.65 V for Pt₁₀₀ NCs, 0.69 V for Pt₇₅Ni₂₅ NCs, 0.73V for Pt₆₇Ni₃₃ NCs, 0.66 V for Pt₅₀Ni₅₀ NCs, 0.67 V for Pt₃₃Ni₆₇ NCs and 0.60 V for Ni₁₀₀ NPs. The results suggest that Pt₆₇Ni₃₃ NCs possessed the best activity among the series, Pt₁₀₀ NCs exhibited moderate activity while Ni₁₀₀ NPs possessed the lowest activity.

Consistent results were obtained in RRDE voltammograms in **Figure 3b**. One can see that the kinetic current density at 2500 rpm at is 4.4 mA cm⁻² for Pt₁₀₀ NCs, 4.8 mA cm⁻² for Pt₇₅Ni₂₅ NCs, 6.5 mA cm⁻² for Pt₆₇Ni₃₃ NCs, 3.9 mA cm⁻² for Pt₅₀Ni₅₀ NCs, 3.5 mA cm⁻² for Pt₃₃Ni₆₇ NCs and 3.1 mA cm⁻² for Ni₁₀₀ NPs. Again, Pt₆₇Ni₃₃ NCs possessed the highest kinetic current density among the series.

Based on the RRDE measurements, the electron transfer number (n) and yield of H₂O₂ during ORR could be calculated according to the following equations:[47, 48]

$$n = \frac{4I_d}{I_d + \frac{I_r}{N}} \quad (1)$$

$$\text{H}_2\text{O}_2 = \frac{200I_r/N}{\frac{I_r}{N} + I_d} \quad (2)$$

where I_d is the disk current, I_r is the ring current, and N is the RRDE collection efficiency (0.37). The n values and H₂O₂ yield v for the different catalysts are presented in **Figure 3c**. For Ni₁₀₀ NPs and Pt₃₃Ni₆₇ NCs, the n value was approximately 3.1 within the potential range of 0 to +0.6 V, indicating that the reaction probably proceeded by a combined two- and four-electron reduction pathways. The n values of Pt₁₀₀ NCs and Pt₇₅Ni₂₅ NCs were somewhat higher at 3.53-3.70 and 3.48-3.70 in the same potential range, and the highest n value was 3.55-3.73 of Pt₆₇Ni₃₃ NCs. Correspondingly, Ni₁₀₀ NPs exhibited the highest yield of H₂O₂, which was about 41% in the potential range of 0 to +0.6 V. For all the alloyed NCs and Pt₁₀₀ NCs, the H₂O₂ yield ranged from 14.6-34.5%, while Pt₆₇Ni₃₃ NCs possessed the lowest value of 14.6-23.4%.

3.4. Further ORR comparison with Pt/C and ECSA analysis

The ORR activity of Pt₆₇Ni₃₃ NCs is further compared with Pt/C. As shown in **Figure S4a**, whereas only featureless charging current was observed in N₂-saturated 0.1 M KOH within the potential range from -0.04 V to +1.16 V, while in O₂-saturated 0.1 M KOH solution, a cathodic peak can be readily identified, indicating valid electrocatalytic activity toward ORR for both Pt₆₇Ni₃₃ NCs and Pt/C. From the LSV curves in **Figure S4b**, one can see the onset potential of Pt₆₇Ni₃₃ NCs is 0.92 V, slightly lower than Pt/C (0.96 V). However, as shown in **Figure S4c**, the number of electron

transfer for Pt₆₇Ni₃₃ NCs (3.56-3.75) is close to Pt/C (3.74-3.91), while the yield of H₂O₂ for Pt₆₇Ni₃₃ NCs is larger than Pt/C correspondingly.

Figure 4a presents the RRDE voltammograms of ORR acquired with the Pt₆₇Ni₃₃ NCs modified electrode in an O₂-saturated 0.1 M KOH solution at different rotation rates (from 100-2500 rpm). The voltammetric currents increased with the increasing of electrode rotation rate. The homologous Koutecky-Levich (K-L) plots (**Figure 4b**) in the potential range of +0.64 to +0.76 V exhibit great linearity with a very consistent slope, suggesting first order reaction kinetics for ORR with regard to oxygen concentration.

Furthermore, the corresponding Tafel plots are shown in **Figure 4c**, the Tafel slopes typically possessed two values at 60 or 120 mV dec⁻¹, in which the former value reflects that a pseudo-two-electron reaction is the rate-determining step. The latter value implies that the reaction rate is governed by the first-electron reduction of oxygen, while the following reduction and O-O bond-breaking process are relatively fast. The Tafel slopes here were calculated as 61.8 mV dec⁻¹ for Pt₆₇Ni₃₃ NCs and 60.2 mV dec⁻¹ for Pt/C in a low overpotential regime (E > +0.89 V), indicating that the reaction mechanism on the surface of these samples were identical with Pt/C, that is, the ORR reaction is probably a pseudo-two-electron reduction process.[12, 14, 49, 50] Meanwhile, the Tafel slope below the potential of +0.85 V was calculated as 109.8 mV dec⁻¹ for Pt₆₇Ni₃₃ NCs, and 121.3 mV dec⁻¹ for Pt/C, indicating that the reaction rate was limited by the first electron transfer to oxygen molecules to some extent.[51-53] To unravel the physical causes for the different ORR activity of the PtNi alloyed NCs, the electrochemically active surface area (ECSA) tests were conducted.[54] **Figure S5** presents the CV curves of all the samples in a N₂-saturated 0.1 M HClO₄ solution. The ECSA value of each sample can be calculated by[22]

$$\text{ECSA}[\text{cm}^2] = Q [\mu\text{C}]/A \quad (3)$$

Where A is the quantity of electricity per unit area for polycrystalline Pt (210 μC cm⁻²). The ECSA values are summarized in **Table 1**. The sample of Pt₆₇Ni₃₃ NCs exhibited the highest ECSA value among the series. In addition, based on the ECSA values, the specific activity (SA) at 0.6 V of all samples was further calculated. From **Table 1**, one can see that, Pt₆₇Ni₃₃ NCs possessed the highest SA value (0.61 mA/cm²), which is quite close to that of commercial Pt/C (0.62 mA/cm²).

It is worth noting that, Pt₆₇Ni₃₃ NCs possessed higher ORR activity than Pt₁₀₀ NCs or Ni₁₀₀ NPs as well as other alloyed samples. It can be probably accounted for the following factors. First of all, the ultrasmall bi-metallic nanoclusters not only impart large effective surface area, but also demonstrated robust stability which is not prone to dissolution, decomposition and aggregation,[52, 55-57] unlike Pt/C. Secondly and more importantly, the synergistic effects between Pt and Ni upon electronic landscape not only facilitate the O-O bonding splitting, but also counterbalances the strong adsorption of O₂ molecules with relatively weak adsorption of poisoning intermediates.[15, 19, 20, 28-30, 34, 43, 58-60]

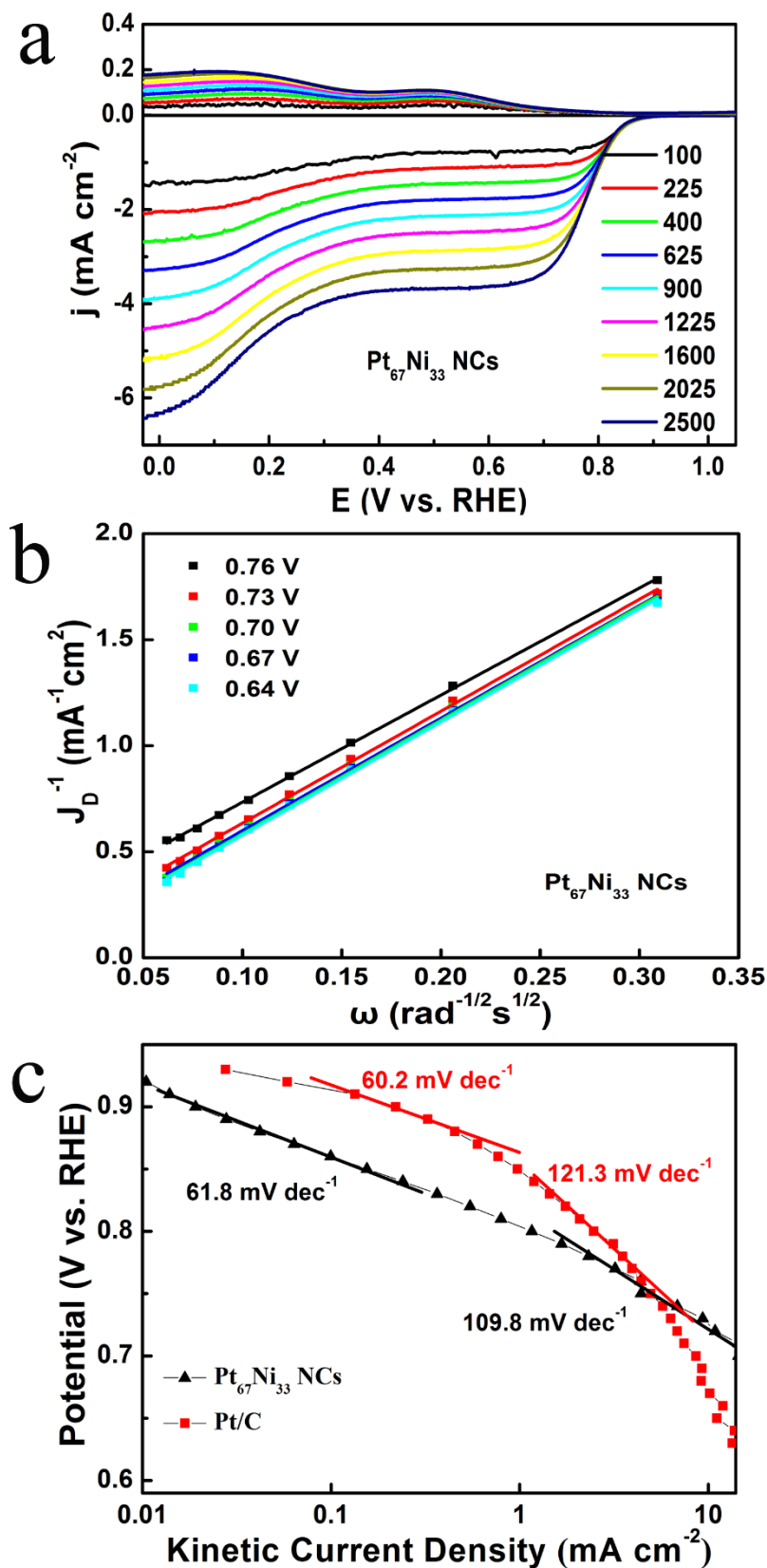


Figure 4. (a) LSV curves for Pt₆₇Ni₃₃ NCs at the rotation rates from 100 to 2500 rpm. (b) The corresponding Koutecky-Levich (K-L) plots for Pt₆₇Ni₃₃ NCs at different potentials. (c) The corresponding Tafel plots of Pt₆₇Ni₃₃ NCs and Pt/C. The potential scan rate is 10 mV s⁻¹ for all measurements.

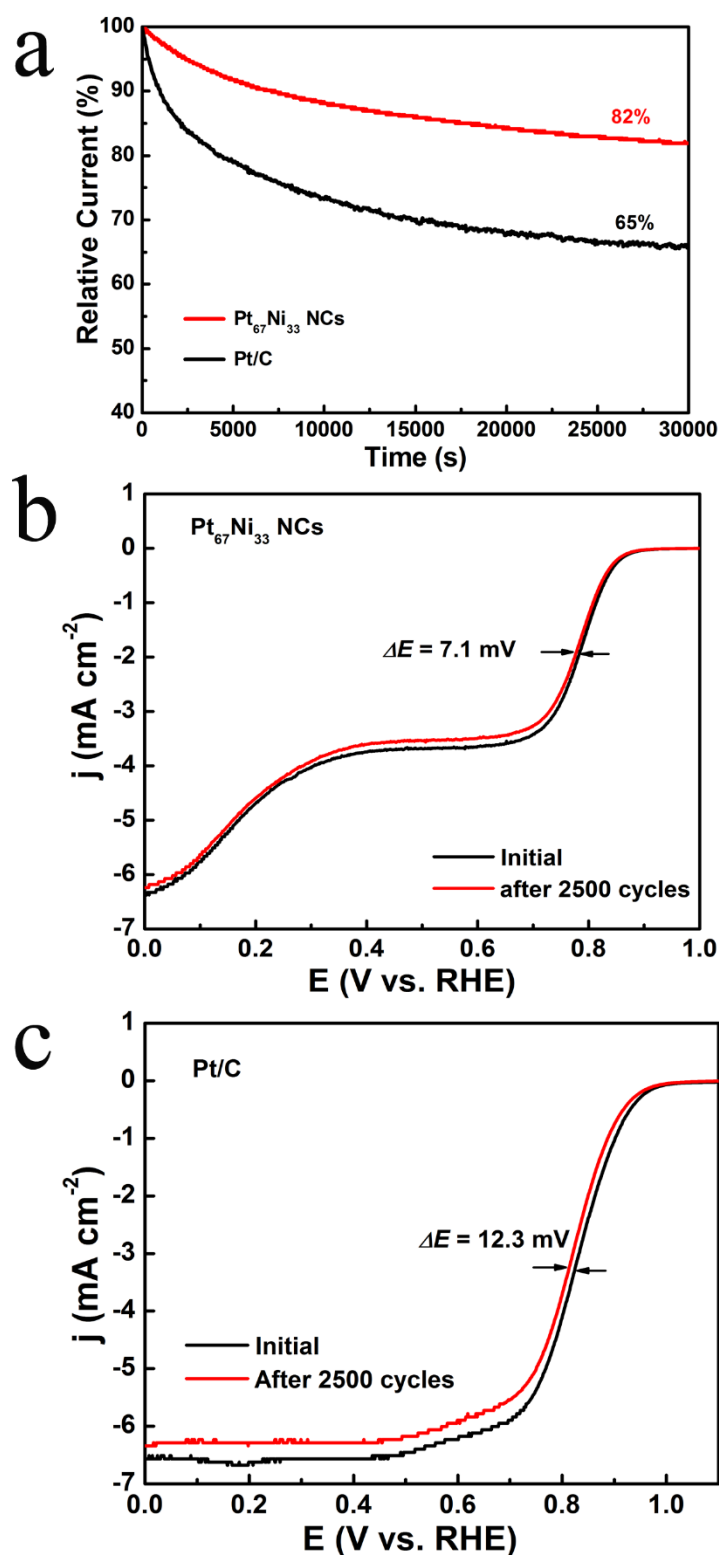
3.5. Long-term durability of Pt₆₇Ni₃₃ NCs compared with Pt/C

Figure 5. (a) Chronoamperometric responses for ORR at Pt₆₇Ni₃₃ NCs and Pt/C electrodes in an O₂-saturated 0.1 M KOH solution at +0.5 V for 30,000 s. The accelerated durability tests of Pt₆₇Ni₃₃ NCs (b) and Pt/C (c) were conducted by before and after 2500 cycles in the potential range of 0.6–1.0 V at a scan rate of 50 mV s⁻¹ with a rotation speed of 2500 rpm in an oxygen-saturated 0.1 M KOH solution.

The chronoamperometric measurements were first conducted to evaluate the long-term durability of Pt₆₇Ni₃₃ NCs and compared with Pt/C.[61] As shown in **Figure 5a**, after more than 30, 000 s continuous operation, the cathodic current of Pt/C exhibited a loss of 35% compared to the initial value. However, the cathodic current of Pt₆₇Ni₃₃ NCs maintained about 82% of its initial value (18% loss). The much lower current attenuation (18% versus 35% of Pt/C) suggests that Pt₆₇Ni₃₃ NCs possessed much higher long-term durability than Pt/C in alkaline solution.

To further assess the durability of the Pt₆₇Ni₃₃ NCs, accelerated durability tests were carried out by cycling the catalyst over the potential range from +0.6 to 1.0 V at 50 mV s⁻¹ in an O₂-saturated 0.1 M KOH solution.[62] As presented in **Figure 5b**, the half-wave potential of Pt₆₇Ni₃₃ NCs shifted negatively only 7.1 mV after 2500 cycles, while commercial Pt/C exhibited a much greater negative shift of 12.3 mV (**Figure 5c**), further attesting the Pt₆₇Ni₃₃ NCs exhibited exceedingly higher durability than Pt/C.

4. CONCLUSIONS

In this work, PtNi alloyed nanoclusters were synthesized and employed as efficient electrocatalyst for ORR. PtNi nanoclusters were synthesized through a wet chemical approach, while the structure and composition of the alloys were modulated by the variation of Pt-to-Ni ratio. Among a series of samples, the sample of Pt₆₇Ni₃₃ NCs stood out as the best sample, superior than the monometallic nickel nanoparticles and platinum nanoclusters as well as other alloyed clusters, in terms of onset potential, kinetic current density, and durability. The ORR performance of Pt₆₇Ni₃₃ NCs was close to Pt/C, as similar specific activity and markedly higher long-term stability were obtained. The findings demonstrated that ultrasmall bi-metallic nanoclusters hold great potential as efficient electrocatalyst for fuel cell applications.

SUPPLEMENTARY MATERIAL

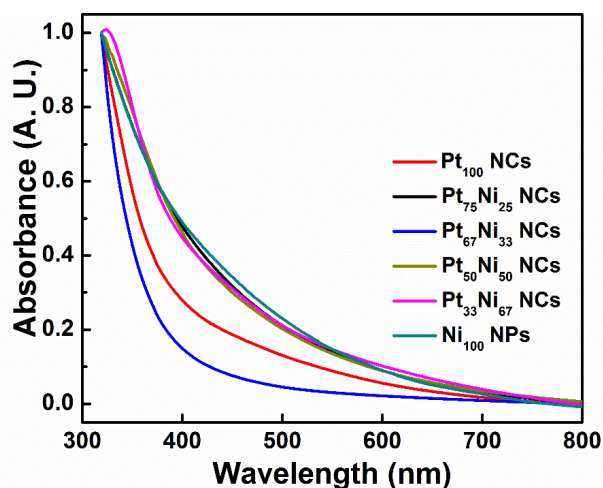


Figure S1. UV-visible absorbance of the PtNi alloyed NCs.

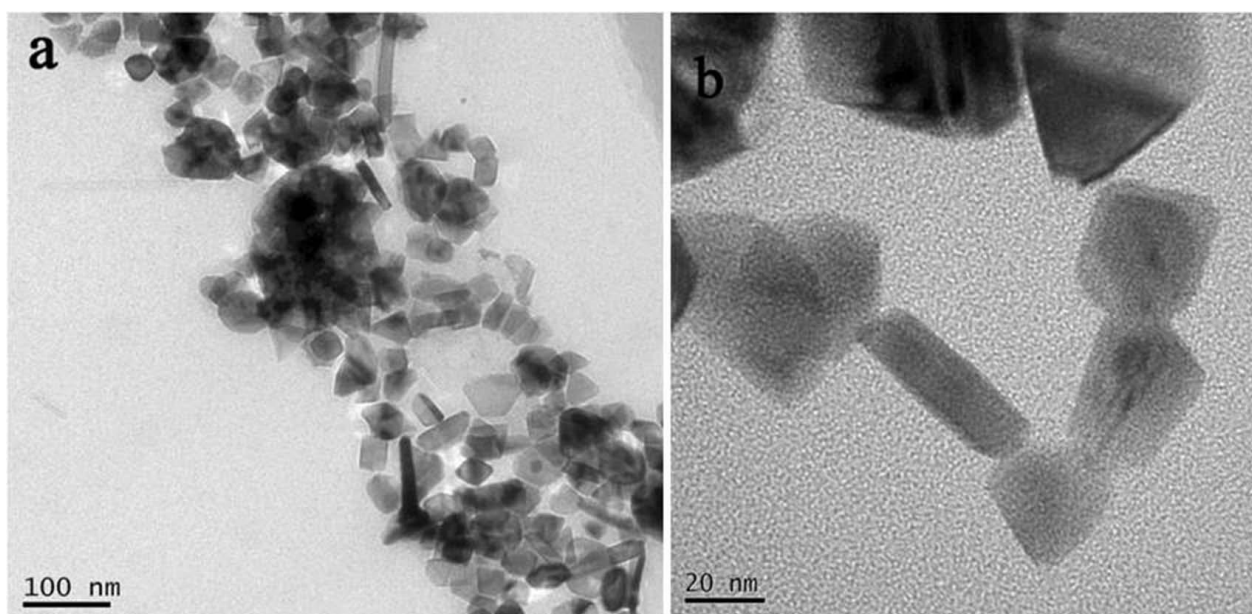


Figure S2. Representative TEM images of nickel nanoparticles with two magnitudes, (a) 100 nm, (b) 20 nm.

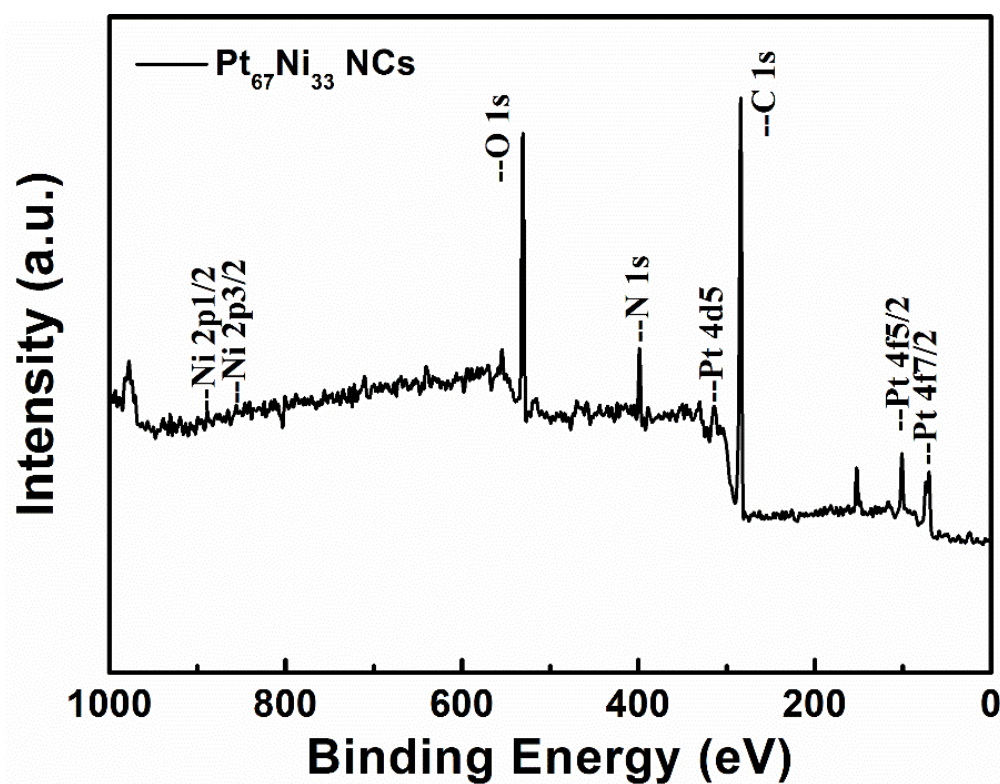


Figure S3. XPS survey spectra of the purified Pt₆₇Ni₃₃ NCs.

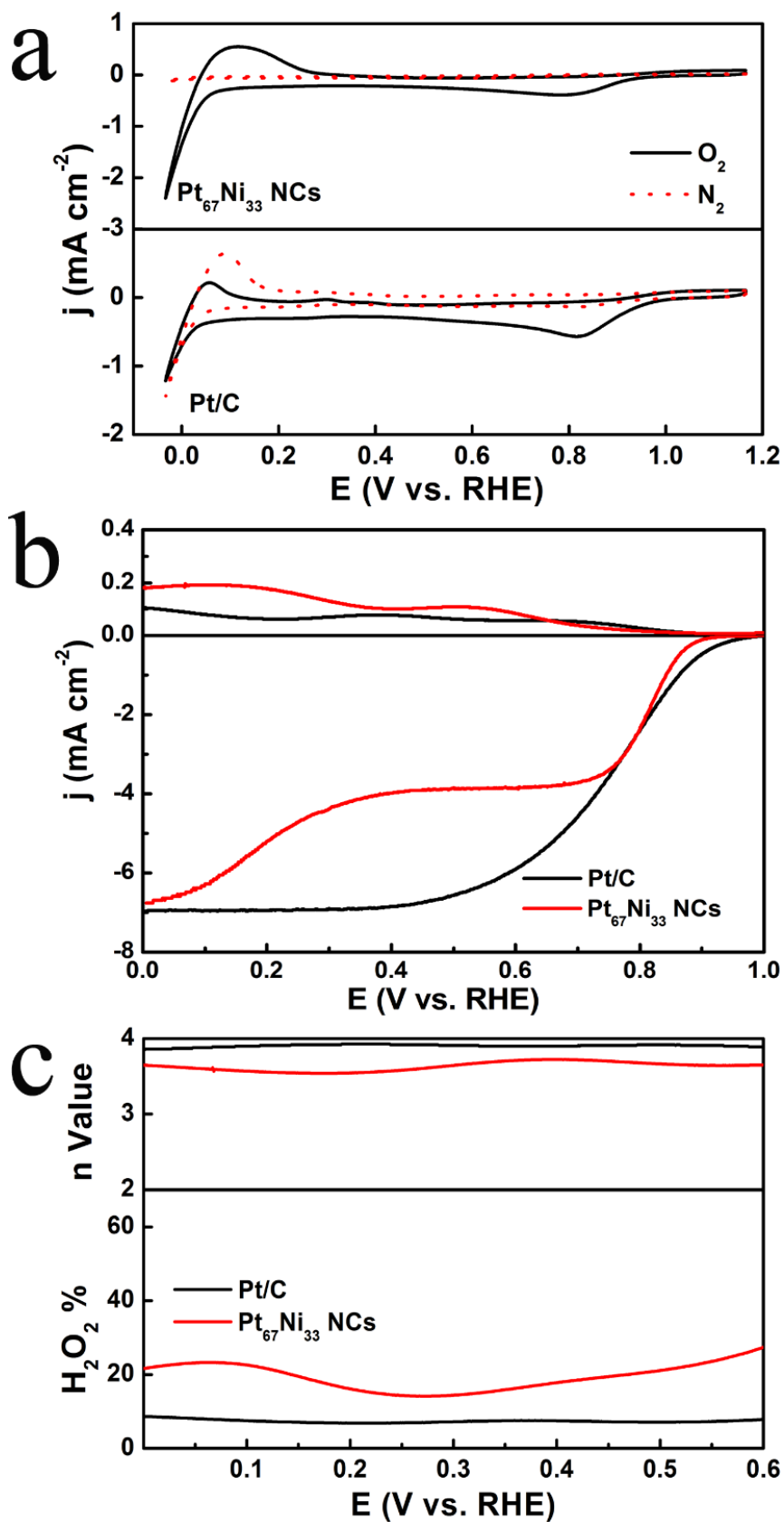


Figure S4. (a) Cyclic and (b) RRDE voltammograms, (c) plots of H₂O₂ yield and electron transfer number of a glassy carbon electrode modified with Pt₆₇Ni₃₃ NCs and Pt/C in O₂-saturated 0.1 M KOH solution. All measurements were conducted at a potential scan rate of 10 mV s⁻¹.

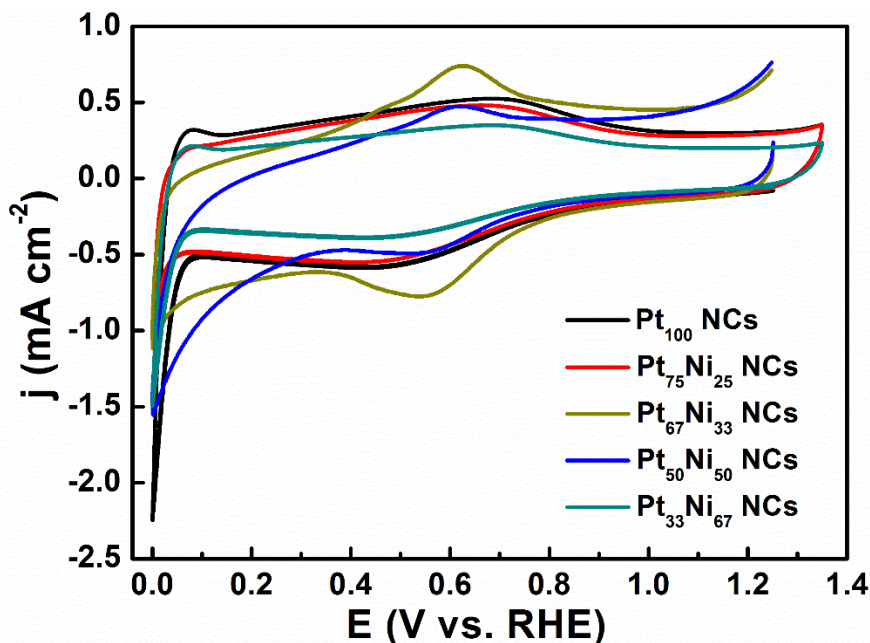


Figure S5. Cyclic voltammograms measured in a N_2 -saturated 0.1 M HClO_4 solution. The measurements were conducted at a potential scan rate of 50 mV s^{-1} .

ACKNOWLEDGEMENTS

W. H. thanks the financial support from Science and Technology Program of Chongqing Teaching Committee (No. KJ1604301), Z. T. acknowledges the support from Guangdong Innovative and Entrepreneurial Research Team Program (No. 2014ZT05N200), and Guangdong Natural Science Funds for Distinguished Young Scholars (No. 2015A030306006).

References

1. M.K. Debe, *Nature*, 486 (2012) 43.
2. A. Kraysberg, Y. Ein-Eli, *Energy Fuels*, 28 (2014) 7303.
3. M. Winter, R.J. Brodd, *Chem. Rev.*, 104 (2004) 4245
4. A.A. Gewirth, M.S. Thorum, *Inorg. Chem.*, 49 (2010) 3557.
5. K.E. Swider-Lyons, S.A. Campbell, *J Phys Chem Lett*, 4 (2013) 393.
6. S. Guo, S. Zhang, S. Sun, *Angew. Chem., Int. Ed.*, 52 (2013) 8526.
7. C.-H. Cui, S.-H. Yu, *Acc. Chem. Res.*, 46 (2013) 1427.
8. B. Lim, M. Jiang, P.H.C. Camargo, E.C. Cho, J. Tao, X. Lu, Y. Zhu, Y. Xia, *Science*, 324 (2009) 1302.
9. Y. Jiao, Y. Zheng, M. Jaroniec, S.Z. Qiao, *Chem. Soc. Rev.*, 44 (2015) 2060.
10. B. Genorio, R. Subbaraman, D. Strmcnik, D. Tripkovic, V.R. Stamenkovic, N.M. Markovic, *Angew. Chem., Int. Ed.*, 50 (2011) 5468.
11. M. Oezaslan, F. Hasché, P. Strasser, *J Phys Chem Lett*, 4 (2013) 3273.
12. M. Liu, R. Zhang, W. Chen, *Chem. Rev.*, 114 (2014) 5117.
13. S. Liu, N. Tian, A.-Y. Xie, J.-H. Du, J. Xiao, L. Liu, H.-Y. Sun, Z.-Y. Cheng, Z.-Y. Zhou, S.-G. Sun, *J. Am. Chem. Soc.*, 138 (2016) 5753.
14. M. Shao, Q. Chang, J.-P. Dodelet, R. Chenitz, *Chem. Rev.*, 116 (2016) 3594.
15. C. Wang, N.M. Markovic, V.R. Stamenkovic, *ACS Catal.*, 2 (2012) 891.
16. T. Kaito, H. Tanaka, H. Mitsumoto, S. Sugawara, K. Shinohara, H. Ariga, H. Uehara, S. Takakusagi, K. Asakura, *J. Phys. Chem. C*, 120 (2016) 11519.

17. V. Čolić, A.S. Bandarenka, *ACS Catal.*, 6 (2016) 5378.
18. Z. Tang, W. Wu, K. Wang, *Catalysts*, 8 (2018) 65.
19. C. Cui, L. Gan, H.-H. Li, S.-H. Yu, M. Heggen, P. Strasser, *Nano Lett.*, 12 (2012) 5885.
20. X. Huang, E. Zhu, Y. Chen, Y. Li, C.-Y. Chiu, Y. Xu, Z. Lin, X. Duan, Y. Huang, *Adv. Mater.*, 25 (2013) 2974.
21. L. Bu, S. Guo, X. Zhang, X. Shen, D. Su, G. Lu, X. Zhu, J. Yao, J. Guo, X. Huang, *Nat. Commun.*, 7 (2016) 11850.
22. L. Wang, Z. Tang, W. Yan, Q. Wang, H. Yang, S. Chen, *J. Power Sources*, 343 (2017) 458.
23. P. Strasser, S. Koh, T. Anniyev, J. Greeley, K. More, C. Yu, Z. Liu, S. Kaya, D. Nordlund, H. Ogasawara, M.F. Toney, A. Nilsson, *Nat. Chem.*, 2 (2010) 454.
24. D.Y. Chung, S.W. Jun, G. Yoon, S.G. Kwon, D.Y. Shin, P. Seo, J.M. Yoo, H. Shin, Y.-H. Chung, H. Kim, B.S. Mun, K.-S. Lee, N.-S. Lee, S.J. Yoo, D.-H. Lim, K. Kang, Y.-E. Sung, T. Hyeon, *J. Am. Chem. Soc.*, 137 (2015) 15478.
25. R.C. Koffi, C. Coutanceau, E. Garnier, J.M. Léger, C. Lamy, *Electrochim. Acta*, 50 (2005) 4117.
26. V.R. Stamenkovic, B.S. Mun, M. Arenz, K.J.J. Mayrhofer, C.A. Lucas, G. Wang, P.N. Ross, N.M. Markovic, *Nat. Mater.*, 6 (2007) 241.
27. V. Stamenkovic, B.S. Mun, K.J.J. Mayrhofer, P.N. Ross, N.M. Markovic, J. Rossmeisl, J. Greeley, J.K. Nørskov, *Angew Chem., Int. Ed.*, 45 (2006) 2897.
28. V.R. Stamenkovic, B. Fowler, B.S. Mun, G. Wang, P.N. Ross, C.A. Lucas, N.M. Marković, *Science*, 315 (2007) 493.
29. J. Zhang, H. Yang, J. Fang, S. Zou, *Nano Lett.*, 10 (2010) 638.
30. C. Wang, M. Chi, D. Li, D. van der Vliet, G. Wang, Q. Lin, J. F. Mitchell, K.L. More, N.M. Markovic, V.R. Stamenkovic, *ACS Catal.*, 1 (2011) 1355.
31. X. Huang, Z. Zhao, L. Cao, Y. Chen, E. Zhu, Z. Lin, M. Li, A. Yan, A. Zettl, Y.M. Wang, X. Duan, T. Mueller, Y. Huang, *Science*, 348 (2015) 1230.
32. N.N. Kariuki, W.J. Khudhayer, T. Karabacak, D.J. Myers, *ACS Catal.*, 3 (2013) 3123.
33. C. Zhang, S.Y. Hwang, A. Trout, Z. Peng, *J. Am. Chem. Soc.*, 136 (2014) 7805.
34. K. Eid, H. Wang, V. Malgras, Z.A. Allothman, Y. Yamauchi, L. Wang, *Chem. Asian J.*, 11 (2016) 1388.
35. R.W. Murray, *Chem. Rev.*, 108 (2008).
36. S. Wang, H. Yu, M. Zhu, *Sci. China Chem.*, 59 (2016) 206.
37. Y. Lu, W. Chen, *Chem. Soc. Rev.*, 41 (2012) 3594.
38. H. Borchert, D. Fenske, J. Kolny-Olesiak, J. Parisi, K. Al-Shamery, M. Bäumer, *Angew Chem., Int. Ed.*, 46 (2007) 2923.
39. R. Bhandari, D.B. Pacardo, N.M. Bedford, R.R. Naik, M.R. Knecht, *J. Phys. Chem. C*, 117 (2013) 18053.
40. Y. Bing, H. Liu, L. Zhang, D. Ghosh, J. Zhang, *Chem. Soc. Rev.*, 39 (2010) 2184.
41. K. Yamamoto, T. Imaoka, W.-J. Chun, O. Enoki, H. Katoh, M. Takenaga, A. Sonoi, *Nat. Chem.*, 1 (2009) 397.
42. P. Lu, T. Teranishi, K. Asakura, M. Miyake, N. Toshima, *J. Phys. Chem. B*, 103 (1999) 9673.
43. K.-H. Choi, Y. Jang, D.Y. Chung, P. Seo, S.W. Jun, J.E. Lee, M.H. Oh, M. Shokouhimehr, N. Jung, S.J. Yoo, Y.-E. Sung, T. Hyeon, *Chem. Commun.*, 52 (2016) 597.
44. R. Jin, C. Zeng, M. Zhou, Y. Chen, *Chem. Rev.*, 116 (2016) 10346.
45. I.A. Khan, Y. Qian, A. Badshah, M.A. Nadeem, D. Zhao, *ACS Appl. Mater. Interfaces*, 8 (2016) 17268.
46. B. Singh, L. Murad, F. Laffir, C. Dickinson, E. Dempsey, *Nanoscale*, 3 (2011) 3334.
47. Q. Wang, Z. Tang, L. Wang, H. Yang, W. Yan, S. Chen, *ChemistrySelect*, 1 (2016) 6044.
48. W. Wu, Z. Tang, K. Wang, Z. Liu, L. Li, S. Chen, *Electrochim. Acta*, 260 (2018) 168.
49. M. Luo, S. Guo, *Nat. Rev. Mater.*, 2 (2017) 17059.
50. G. Wu, J. Wang, W. Ding, Y. Nie, L. Li, X. Qi, S. Chen, Z. Wei, *Angew Chem., Int. Ed.*, 55 (2016)

- 1340.
51. G. He, Y. Song, K. Liu, A. Walter, S. Chen, S. Chen, *ACS Catal.*, 3 (2013) 831.
 52. L. Wang, Z. Tang, W. Yan, H. Yang, Q. Wang, S. Chen, *ACS Appl. Mater. Interfaces*, 8 (2016) 20635.
 53. L. Wang, Z. Tang, X. Liu, W. Niu, K. Zhou, H. Yang, W. Zhou, L. Li, S. Chen, *RSC Adv.*, 5 (2015) 103421.
 54. Y. Li, W. Gao, L. Ci, C. Wang, P.M. Ajayan, *Carbon*, 48 (2010) 1124.
 55. W. Tang, H. Lin, A. Kleiman-Shwarsctein, G.D. Stucky, E.W. McFarland, *J. Phys. Chem. C*, 112 (2008) 10515.
 56. Q. Wang, L. Wang, Z. Tang, F. Wang, W. Yan, H. Yang, W. Zhou, L. Li, X. Kang, S. Chen, *Nanoscale*, 8 (2016) 6629.
 57. N. Li, Z. Tang, L. Wang, Q. Wang, W. Yan, H. Yang, S. Chen, C. Wang, *RSC Adv.*, 6 (2016) 91209.
 58. V. Beermann, M. Gocyla, E. Willinger, S. Rudi, M. Heggen, R.E. Dunin-Borkowski, M.-G. Willinger, P. Strasser, *Nano Lett.*, 16 (2016) 1719.
 59. J. Wu, H. Yang, *Acc. Chem. Res.*, 46 (2013) 1848.
 60. G.A. Attard, A. Brew, J.-Y. Ye, D. Morgan, S.-G. Sun, *ChemPhysChem*, 15 (2014) 2044.
 61. W. Yan, Z. Tang, L. Wang, Q. Wang, H. Yang, S. Chen, *Int. J. Hydrogen Energy*, 42 (2017) 218.
 62. W. Yan, Z. Tang, L. Li, L. Wang, H. Yang, Q. Wang, W. Wu, S. Chen, *ChemElectroChem*, 4 (2017) 1349

© 2018 The Authors. Published by ESG (www.electrochemsci.org). This article is an open access article distributed under the terms and conditions of the Creative Commons Attribution license (<http://creativecommons.org/licenses/by/4.0/>).